JOURNAL OF MATERIALS SCIENCE 4 (1969) 485–498

Exploring the Rôle of Impurities in Non-metallic Materials by Electron Paramagnetic Resonance

T. I. BARRY
Division of Inorganic and Metallic Structure, National Physical Laboratory, Teddington, Middlesex, UK

Received 19 November 1968

In a penetrating review on defects in diamond [1], Frank draws conclusions about the depth, temperature and time scale of its genesis. He writes, "A diamond is a letter to us from the depths . . . but the perfect crystal is a blank page. The individuality of every diamond resides in its imperfections, and these afford our only clue to what has happened to that crystal since its birth."

The present paper advances electron paramagnetic resonance (epr) as a technique for detecting these clues in materials, most of which are more mundane than diamond, and discusses applications to a range of materials problems. It is unfortunate that information in the form of epr spectra is still in a sense encoded, so a secondary aim of this paper is to collect together methods for deciphering the message.

1. Introduction

The aim of this paper is primarily to show how epr can be applied to solving problems concerned with the rôle of impurities in materials. Transition metal ions, most of which can be sensitively detected by epr, are present as impurities or deliberate additives in a wide range of materials and are known to have a strong influence on such processes as crystal nucleation and growth, dislocation and grain-boundary motion, solid state reactions and catalysis, processes which have a direct effect on the generation and application of materials as diverse as gemstones, cement, pigments and refractories.

The solution of impurities in solids is enhanced when the solids are prepared by rapid precipitation or by treatment at high temperatures, whereas at low temperatures solid solubility is reduced and impurity ions tend to be expelled from the lattice. The free energy of the system is lowered if impurity rather than normal lattice ions become associated with existing lattice defects such as vacancies, dislocations or grain-boundaries. Cold working of the specimen or treatment at intermediate temperatures accelerates the process of association of impurities with defects, with the result that grain-boundaries become rich in impurity material [2]. This material may form a skin round the grains or alternatively may aggregate into clumps of a phase rich in impurity ions. In either case the changes in distribution, from complete solid solution through progressive stages of aggregation, have a profound effect on the physical, chemical and mechanical properties of solids [3].

It is less easy to give a summary of the behaviour of impurities during hydrolytic processes such as the conversion of clinker to cement or of clays to earthenware and porcelain. But in these materials too, minor constituents have an important influence [4].

Epr makes it possible to trace the progress of impurities and to correlate their distribution with changes in other properties. The types of information which can be deduced are listed below.

(*a*) The identity and valence of the paramagnetic ions.

(*b*) The local symmetry and environment of the

centres and hence the nature of the phase giving rise to that environment, changes caused by neighbouring defects, solid solution of other ions, lattice strain, etc.
(*c*) The overall concentration of the centres.
(*d*) The local concentration of the centres. Proximity of paramagnetic centres gives rise to line broadening through spin dipole interaction. The occurrence of magnetic exchange interaction can give detailed information on the mutual location of centres and on the nature of magnetically concentrated phases.

Most epr equipments have facilities for study down to 77° K but not to lower temperatures. This being so it is usually possible to obtain spectra only from ions in the first transition series which have odd numbers of unpaired electrons. Thus the most convenient ions for study are Ti^{3+}, V^{4+}, Cr^{5+}, Cu^{2+}; V^{2+}, Cr^{3+}, Mn^{4+}; Mn^{2+} and Fe^{3+}. Fortunately these ions include many of the important impurities. Review articles on transition metal ions have been provided by Carrington and Longuet-Higgins [5] (introduction to theory), Low and Offenbacher [6] (data), Kokoszka and Gordon [7], König [8] and Orton [9]. Reference is given in these reviews to other collections of data. The book by Orton [9] also covers other transition and rare earth ions.

Unfortunately, the interpretation of epr spectra is not straightforward, especially for polycrystalline or amorphous specimens, so a secondary aim of the paper is to refer the reader to methods of analysis. For this reason the framework of section 3 will be a guide to the factors which influence the spectra, and this framework will be used as the context for illustrations of applications to materials science. Applications to optical, electrical and magnetic materials will not be accentuated, because for these materials the rôle of the transition metal ions is more obvious. The important field of radiation-induced paramagnetic centres will also be largely neglected.

A problem frequently encountered within all disciplines is that it is often very difficult to gauge the credibility of a piece of work which uses an unfamiliar physical technique such as epr to obtain structural information. Moreover, the epr specialist may be unfamiliar with the chemistry and physics of the system he is studying and for that reason may make incorrect deductions. It is hoped that this paper may provide a bridge between those most concerned with theoretical aspects of epr and those who may be interested in applying it to materials problems. Certainly a beginner will wish to make his first essays into epr under the wing of someone more experienced.

2. Possible Applications of EPR

2.1. Isolated Ions

2.1.1. Identification

Epr has value specifically when information is desired about the valence state and location of impurities in the matrix; it is not suitable for conventional analysis. Epr is non-destructive and has an advantage in this respect, provided the specimen will enter the microwave cavity, i.e. for examination at X-band frequencies (9 to 10 GHz), it must be small enough to be contained within a cylinder 11 mm in diameter and of indefinite length.

Identification of ions is achieved through a knowledge of the factors which determine the spectrum. In section 3 of this paper, these factors are dealt with and formulae are given which enable spectra to be compared with existing data.

2.1.2. Symmetry

One of the most powerful uses of epr arises from the information it gives about the symmetry and orientation of paramagnetic centres. For example in rutile (TiO_2), transition metal ions can occupy either substitutional or interstitial sites. For single crystals, the types of sites occupied can be discovered by rotation of the specimen about its four-fold axis, while this is held perpendicular to the magnetic field of the spectrometer. For the substitutional centres, the spectra divide into two sets which are alike, but 90° of rotation out of phase. These two sets have symmetry about the 110 directions of the rutile. On the other hand, the spectra from ions in interstitial sites divide into four sets, which have symmetry axes 5 to 20° either side of the 110 directions. The angle depends on the ion in question. The important point to note is that the distinction between the two types of sites is derived, not from the use of any theoretical treatment, but simply by comparison of the symmetry of the spectrum with the symmetry of possible sites in the rutile structure [10].

Now that much data is available for transition metal ions in single crystals [6], it is possible to use this information to identify their environment in polycrystalline materials. In the absence

of such data, the symmetry deduced from the spectrum can still be a guide. For example, a specimen of chemically pure rutile (TiO_2) doped with 100 ppm Cr^{3+} gave rise, not only to the normal spectrum, which showed the Cr^{3+} to be in orthorhombic sites, consistent with the D_{2h} (*mmm*) point symmetry of the Ti^{4+} sites, but also to a spectrum showing Cr^{3+} in axial symmetry, quite incompatible with the rutile structure. The logical deduction was that the specimens contained a proportion of anatase, a metastable phase of TiO_2, in which the Ti^{4+} sites have S_4 ($\bar{4}$) symmetry [11]. It would have been possible to detect approximately 0.02% of anatase in this way assuming the Cr^{3+} to have been uniformly distributed.

2.1.3. Stress

Both hydrostatic [12] and anisotropic [13] stresses induce changes in the epr spectra of paramagnetic ions, the effect of uniaxial stress being the most obvious since epr is most sensitive to distortions from cubic symmetry. The mathematical treatment and scope of epr for determining internal strains has been reviewed in a series of articles by Stoneham [14]. The order of magnitude for the limits of detection of strains and other defects in MgO are listed as follows: strains 10^{-4}; electric fields 10^5 V/cm; dislocation density 10^6 cm^{-2}; charged defect concentration 11 ppm for singly charged defects and 4 ppm for doubly charged defects. Possible further applications lie in the determination of local strain in crystals deformed by plastic flow and the measurement of stresses in glasses [15] or ceramics [16] toughened by surface ion exchange.

Wenzel and Kim [17] and Kirkby and Thorp [18] have used epr to determine strain and orientation variations at Cr^{3+} sites in ruby. It proved possible to determine the magnitudes of strains of the order of 10^{-4} in single crystals grown by the Verneuil and Czochralski methods.

2.2. Impurity-defect interactions

Although impurity ions of the same valence as the ions of the host lattice are known to cause substantial changes in mechanical properties [19], the influence of ions of different valency should be much more marked, since these can be incorporated only in conjunction with compensating defects, which are necessary to preserve electrical neutrality. For example, in alkali halides, divalent ion impurities are normally incorporated with an equal number of cation vacancies, which may be dissociated from their impurity ions or associated in pairs or in clusters with them [20, 21]. In a study of this system Pratt and co-workers [22] have found by electrical measurements that cation vacancies located at dislocation cores are compensated remotely by the divalent cations. Nevertheless, the divalent ions are attracted into regions near the dislocations by the negative space charge associated with the cation vacancies, and dislocation motion is impeded by the stress required to overcome this electrostatic interaction.

A second way in which charge compensation can be achieved is by mutual compensation of two impurities. For example, in MgO, Al^{3+} and Li^+ ions provide mutual compensation, or again in MgO, dissolved Ni^{2+} ions tend to become oxidised to Ni^{3+} when Li^+ ions are incorporated. This type of charge manipulation is of far-reaching importance in magnetic materials such as ferrimagnetic spinels, for which the factors affecting the valence and distribution of cations have been closely studied [23, 24]. In silicate materials, Al^{3+} ions replacing the Si^{4+} ions in tetrahedral sites are usually compensated by alkali ions in interstitial positions. The extent of replacement can be very large [25].

From the example of divalent ions in alkali halides it is clear that dislocation and grain boundary motions are critically dependent on impurity content. Thus the high temperature deformation of ceramics should be subject to the control of vacancy concentration by addition of charge compensating ions.

The ways in which epr can be used to examine the interaction of impurity and compensating centres are exemplified by thorough studies of aluminium and germanium centres in α-quartz [26, 27]. During irradiation by X- or γ-rays, Al^{3+} ions trap positive holes and Ge^{4+} ions trap electrons. This transfer of charge causes the alkali ions, which are compensating the charge of Al^{3+} ions, to be repelled by the positive holes, and subsequently to arrive at the Ge^{3+} ions. The presence of the alkali ions can be detected, not only by the changes in the *g*-values but also by the characteristic splitting of the spectra caused by the nuclear spins of K, Na and Li. These studies also provide an excellent example of the technique of using irradiation to make existing lattice defects visible.

Although impurities are known to cause large changes in crystal growth rate and crystal habit,

the mechanism of these changes is obscure. In a study of Fe^{3+} centres in amethyst-quartz, Barry, McNamara and Moore [28] found that under any particular pyramidal growth face, the Fe^{3+} ions did not populate the three equivalent silicon sites equally. Moreover, the mode of incorporation of Fe^{3+} in "Z-cut" synthetic quartz was quite different from Fe^{3+} in amethyst. The same sort of inequalities have also been observed for Gd^{3+} in Al_2O_3 [29] and Fe^{3+} in calcite [30]. Such results, if obtained in the context of a study of the topographical aspects of growing crystals, could be used to clarify the influence of impurities on the growth of single crystals and hence on the use of impurities to control grain growth in polycrystalline materials.

2.3. Aggregation of Impurities

Aggregation of impurities into clusters or into crystallites of a new phase causes precipitation hardening and changes in grain-boundary adhesion and sliding [3]. The nucleation and extent of aggregation can be studied by epr in two ways.

The first method is to add exclusively a paramagnetic impurity to the matrix so that the progressive aggregation of the impurity can be studied through the resultant exchange coupling between the magnetically concentrated ions. The second method uses a diamagnetic impurity with a smaller amount of a similar paramagnetic impurity as a monitor. As monitor ions leave the matrix and enter the newly emergent phase, the epr spectrum of the monitor ions in the new phase provides information on the precipitation of the phase, which may be too poorly developed to provide coherent X-ray diffraction. The first technique has the advantage that only one impurity is present but, on the other hand, interpretation of spectra from clustered paramagnetic ions is more difficult. There are no microscopic techniques capable of resolving the earliest stages of precipitation in solids, whereas, in principle epr can be used to study clusters of atoms from pairs to well-formed crystals. Thus the use of epr in selected systems could resolve some important problems of the early stages of nucleation.

3. Factors Influencing the Spectra

3.1. One Unpaired Electron ($S = 1/2$)

The ions with one unpaired electron are Ti^{3+}, V^{4+}, Cr^{5+}, Ni^{+} and Cu^{2+}.

3.1.1. The g-value

The g-value or spectroscopic splitting factor gives a measure of the orbital contribution to the magnetic moment of unpaired electrons. For pure spin angular momentum $g = 2.00232$, and the deviation from this value can be used to give detailed information on the bonding to surrounding ions, as indicated in the review article by Carrington and Longuet-Higgins [5]. However, in the present paper it will be sufficient to consider g-values simply as parameters to describe centres, much as unit cell dimensions are used to summarise X-ray data. The same principles will be applied to the other parameters, which define nuclear spin coupling, crystal field splitting and exchange effects.

An unpaired electron in a magnetic field can take up orientations with its magnetic moment either parallel or antiparallel to the field. These two states are characterised by their quantum numbers, $M = +1/2$ or $-1/2$, which in the magnetic field are associated with different energies as shown in fig. 1.

Transitions can occur between the two states when the field is adjusted so that the energy difference, $g\beta H$, is equal to the fixed microwave energy $h\nu$. The equation

$$h\nu = g\beta H_0 \qquad (1)$$

defines the field H_0 at which resonance will occur in the absence of perturbations by nuclear spins or crystal field splitting (crystal field splitting

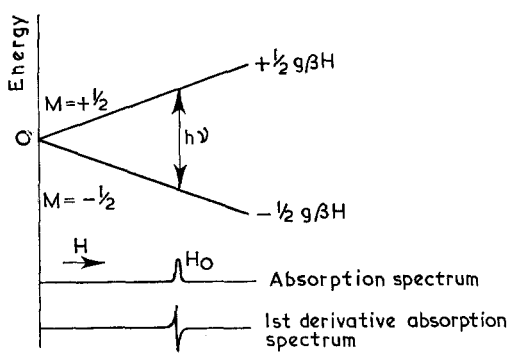

Figure 1 Energy levels of an unpaired electron in a magnetic field. Application of microwave radiation of energy $h\nu$ causes resonance at a field, $H_0 = h\nu/g\beta$.

occurs only if there is more than one unpaired electron).*

In papers on epr it is usual to let frequency and energy have the same units, so that Planck's constant, h = 1. The Bohr Magneton, β, then has a value 1.3996 MHz G^{-1} or 0.46686×10^{-4} cm^{-1} G^{-1}. The g-values which are likely to be observed fall between 2.4 and 1.8. Values for Cu^{2+} are usually greater than 2, values for Ti^{3+}, V^{4+}, Cr^{5+} are usually less than 2. For $g = 2$ and a microwave frequency of 9500 MHz, H_0 is 3394 gauss.

3.1.2. Symmetry and Orientation

If a centre has cubic (O_h, $m3m$ or T, 23) symmetry then its g-value is isotropic. In axial symmetry (minimum point group S_4, $\bar{4}$, or C_3, 3) two extreme values $g_{parallel}$ and $g_{perpendicular}$ are possible and centres with lower symmetry require three orthogonal g-values usually written g_x, g_y and g_z. The g of equation 1 is given by

$$g^2 = g_z^2 \cos^2\theta + g_x^2 \sin^2\theta \cos^2\phi + g_y^2 \sin^2\theta \sin^2\phi \quad (2)$$

where θ and ϕ define the orientation of the magnetic field with respect to the x, y and z co-ordinates of the centre as shown in fig. 2. In axial symmetry $g_z = g_{par}$ and $g_x = g_y = g_{per}$.

Besides affecting the g-values, distortion from cubic symmetry has an important influence on relaxation time, which is briefly discussed in section 3.3.1. The result is that for $3d$ ions with one unpaired electron, the maximum temperature at which epr can be observed decreases with decreasing degree of distortion. Thus the absence of detectable resonance is not a sufficient criterion that such ions are absent. However, reference to existing data will often show whether resonance is likely to be observable for ions in the matrix in question.

For polycrystalline and amorphous materials the spectra obtained are the sums of spectra from ions in all orientations. Fortunately the spectra tend to pile up at certain field values corresponding to orientations of centres having x, y or z axes parallel to the field. The appearance of such spectra for centres with one unpaired electron is now fairly well documented [31-33].

3.1.3. Nuclear Spin Coupling (Hyperfine Structure)

The interaction or coupling of an unpaired electron with the spin of an atomic nucleus causes splitting of the electron states into $(2I + 1)$ energy levels, where I is the nuclear spin. Each level is characterised by a nuclear spin quantum number m which can take values from $-I$ to $+I$. Normally epr transitions are allowed only between energy levels corresponding to the same m and therefore the transitions also are split into $(2I + 1)$ lines. An illustration of the effect of the coupling of an unpaired electron with a nuclear spin of 1/2 is given in fig. 3. Interaction with a single nucleus splits the transition into lines of approximately equal intensity whereas, when

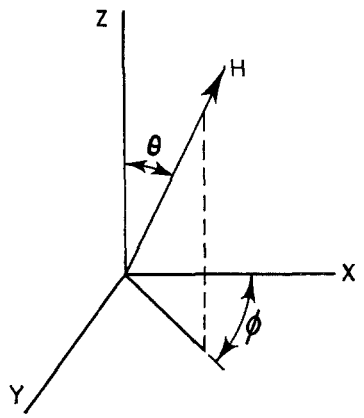

Figure 2 The definition of the angles θ and ϕ, which give the orientation of the magnetic field relative to the symmetry axes of the paramagnetic centre.

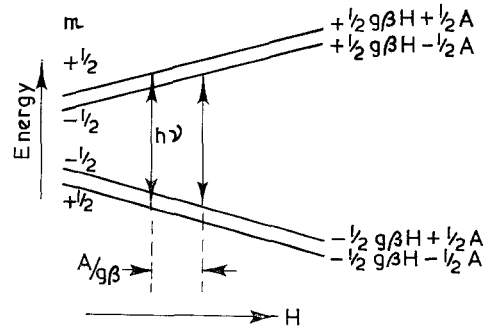

Figure 3 Energy levels of a single unpaired electron interacting with a nucleus of spin 1/2. Second order corrections are omitted. Transitions occur between levels for which there is no change in the nuclear spin quantum number m.

*The g-value is a function of orientation only. Sometimes authors fall into the confusing practice of giving g-values to individual peaks in a spectrum influenced by crystal field splitting. For any one type of centre at any fixed orientation relative to the field, only one g-value, defined by $h\nu = g\beta H_0$ is possible. In the present paper the ratio H/H_0 is used to define the field of individual resonance peaks whose position is a linear function of microwave frequency.

centres interact with several nuclei, each nucleus causes a $(2I + 1)$-fold splitting and transitions commonly overlap to give a binomial intensity distribution among the resolvable peaks. The term hyperfine structure is used to describe the splitting caused by nuclei within the paramagnetic centre; superhyperfine splitting describes splitting by extra-molecular nuclei.

The hyperfine structure is governed by the same symmetry considerations as the g-value. In cubic symmetry, the fields for the $(2I + 1)$ resonance lines are given by

$$H = H_0 - \frac{Am}{g\beta} - \frac{A^2}{2g^2\beta^2 H_0}\{I(I+1) - m^2\} \quad (3)$$

where $H_0 = h\nu/g\beta$ is the field at which reso ıance would occur in the absence of nuclear spin. A is the nuclear spin coupling parameter which is measured in units of energy. The form of equation 3 shows that the spectra will consist of $(2I + 1)$ lines with average separation $A/g\beta$ and increasing separation at the high field end.

The equivalent equation for axial symmetry [34] is complicated by its orientation dependence. However, it is possible to orient single crystals, with the principal symmetry axis of a set of centres parallel or perpendicular to the field. Moreover, spectra from polycrystalline or amorphous specimens are dominated by the contributions from the same orientations.*

The equations for the perpendicular and parallel directions are

$$H_{\text{par}}(m) = H_{0\,\text{par}} - \frac{Am}{g_{\text{par}}\beta} - \frac{B^2}{2(g^2\beta^2 H_0)_{\text{par}}}\{I(I+1) - m^2\} \quad (4)$$

$$H_{\text{per}}(m) = H_{0\,\text{per}} - \frac{Bm}{g_{\text{per}}\beta} - \frac{A^2 + B^2}{4(g^2\beta^2 H_0)_{\text{per}}}\{I(I+1) - m^2\} \quad (5)$$

Here A is the parallel and B the perpendicular nuclear spin coupling parameter. The principal isotope of vanadium, ^{51}V, has a nuclear spin $I = 7/2$ which causes an eight-fold splitting of the spectra. The form of the spectra is represented in fig. 4 by the epr of V^{4+} in polycrystalline Li_2TiSiO_5, [35] which is a tetragonal phase of unknown structure but which clearly has the V^{4+} in sites of axial symmetry, since the perpendicular peaks are not split into x and y components. Note the transition with $m = 1/2$ which is very strong because of the very small orientation dependence of this peak.

Fig. 5 shows a computed spectrum for V^{4+} ions with g, A and line width parameters set to match those for V^{4+} in a glass [35]. The value of computation is that it provides standard spectra for known g and A parameters. These give a check that the correct field positions for the components of experimentally observed spectra are being fed into equations 4 and 5.

The spectra of V^{4+} in sodium borate glasses have been used by Hecht and Johnston [36] to study the nature of the boron oxide anomaly (a discontinuity in the physical properties of borate

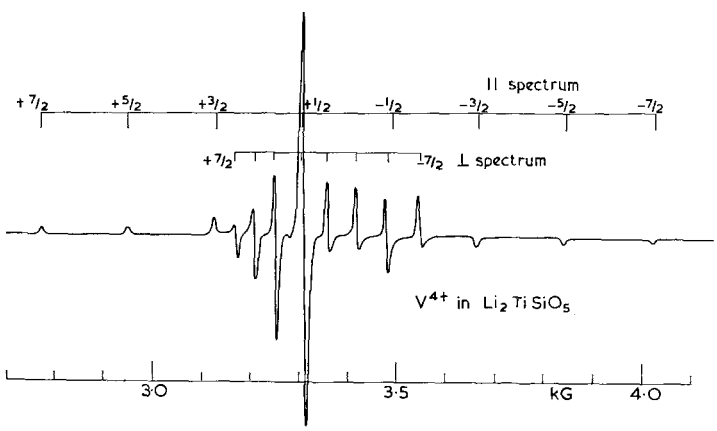

Figure 4 The spectrum of V^{4+} in polycrystalline Li_2TiSiO_5. This phase has an unknown tetragonal structure. The microwave frequency, $\nu = 0.309$ cm^{-1}, $g_{\text{par}} = 1.951$, $g_{\text{per}} = 1.967$, $A = 0.01621$ cm^{-1}, $B = 0.00492$ cm^{-1}.

*This is not always the case. Cu^{2+} and Co^{2+} are particularly liable to give spectra from polycrystalline compounds for which other orientations make important contributions [33, 34].

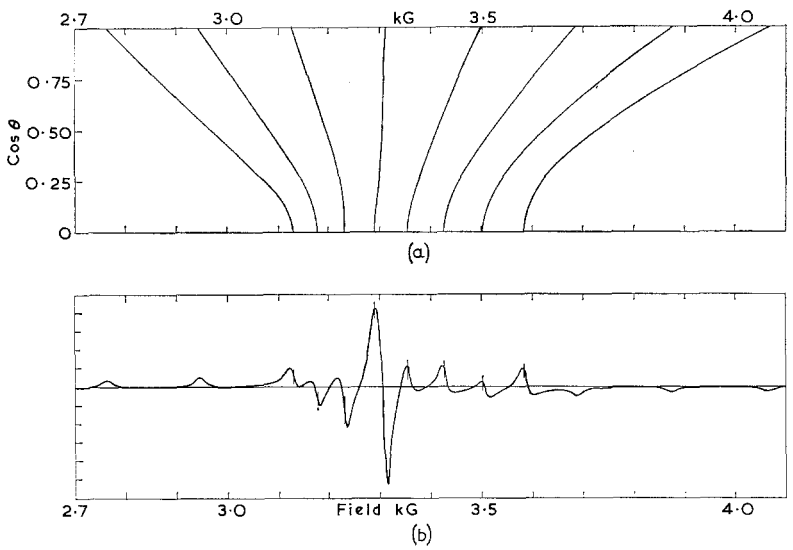

Figure 5(a) The angular variation of the calculated, resonance fields of V^{4+} corresponding to the eight values of m. $\nu = 0.309$ cm^{-1}, $g_{par} = 1.940$, $g_{per} = 1.967$, $A = 0.01680$ cm^{-1}, $B = 0.00594$ cm^{-1}; (b) the computed spectrum corresponding to the angular variation of fig. 5(a). The line width has been chosen to match that in a glass, 15 Gauss (Lorentzian). The greater width of the outer transitions in the experimental spectrum [35] shows that inhomogeneity and not relaxation broadening was responsible for the line width.

glasses as a function of composition). In this case a detailed analysis of the spectra has been made on the basis of ligand field theory, which shows that the V^{4+} ions have one short and four or five longer bonds to give a square-pyramidal structure. The surrounding oxygens are linked only to one boron atom each (the oxygens are said to be non-bridging) and the relative V-O bond lengths have been determined as a function of composition. Results of this type would be difficult to obtain in any other way; they help to put theories of structure in glass on a secure basis.

3.2. Ions with more than one Unpaired Electron

The principal ions of interest within this group are Cr^{3+}, Fe^{3+} and Mn^{2+}. For all of these ions g is isotropic or very nearly so. For Cr^{3+}, g is usually about 1.98, for Fe^{3+} and Mn^{2+}, $g = 2.00$ [6].

3.2.1. Cr^{3+} in Weak Crystal Fields

Cubic symmetry. Cr^{3+} has three unpaired electrons and therefore the electron spin $S = 3/2$. There are four spin states defined by the magnetic quantum number M, which can take the values $+3/2$, $+1/2$, $-1/2$ or $-3/2$. If the crystal field is isotropic the four spin states have energies $Mg\beta H$, which diverge linearly with field and hence the three possible transitions between the four levels superimpose at the field $H_0 = h\nu/g\beta$. However, in the electric field gradient arising from non-cubic surroundings, the energy levels are split even at zero field so that the fields for the transitions are functions of the crystal field and its orientation to the magnetic field. Figs. 6a, b and c show how the energy levels vary with orientation and field for the example of Cr^{3+} in methyl ammonium aluminium sulphate at 77° K, which is discussed further below.

Axial symmetry. If the symmetry is axial and the crystal field effects are weak compared with $g\beta H$, then the transitions $M \Leftrightarrow (M-1)$ occur at fields given by [34]

$$H = H_0 - \frac{D}{g\beta}\left(M - \frac{1}{2}\right)(3\cos^2\theta - 1) + \frac{D^2\cos^2\theta\sin^2\theta}{2g^2\beta^2H_0}\{4S(S+1) - 24M(M-1) - 9\} - \frac{D^2\sin^4\theta}{8g^2\beta^2H_0}\{2S(S+1) - 6M(M-1) - 3\} \quad (6)$$

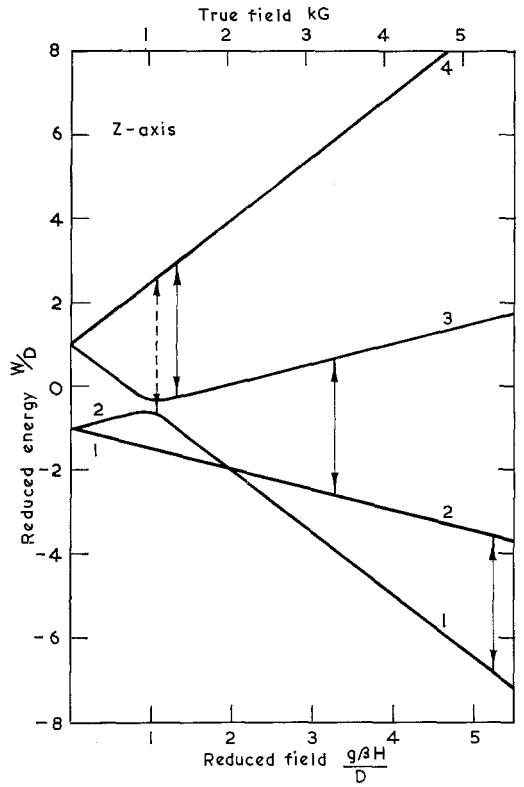

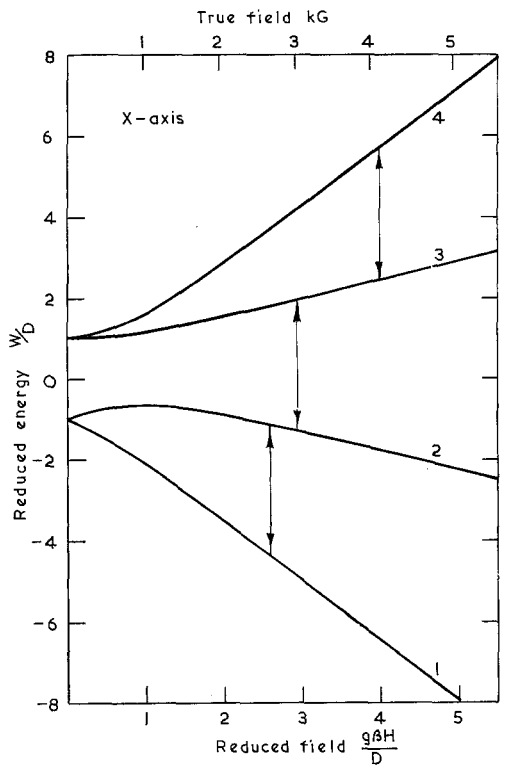

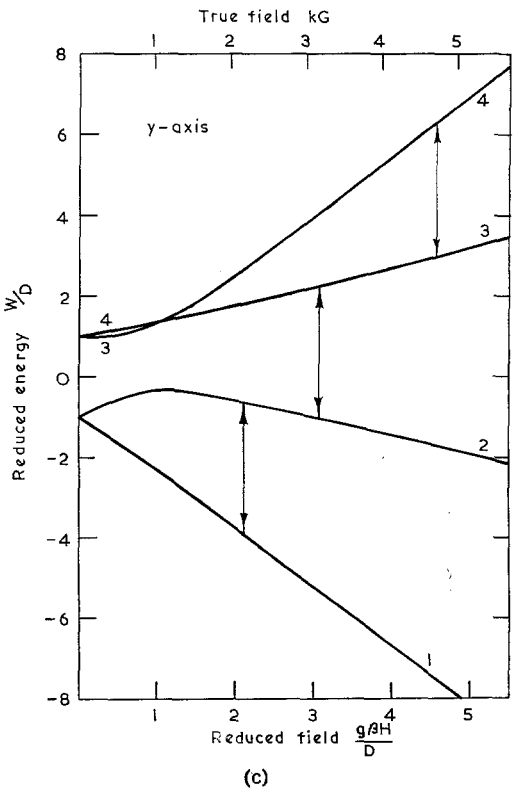

Figure 6(a), (b) and (c).The calculated energy levels for Cr^{3+} substituting for Al^{3+} in $CH_3NH_3Al(SO_4)_2.12H_2O$ at 77° K. $D = 0.095$ cm^{-1}, $E/D = 0.1$, $g = 1.977$. Transitions are marked for a microwave frequency of 0.309 cm^{-1}. (The energy levels have been numbered rather than labelled by quantum numbers, because these become inappropriate at low fields.) Energy is plotted in dimensionless units.

where θ is the angle of the magnetic field to the symmetry axis of the centre, and D represents the strength of the axial electric field gradient measured in energy units. Thus D is a measure of the axial distortion from cubic symmetry.

For polycrystalline specimens the spectrum piles up at fields corresponding to orientations for which the field varies slowly with orientation. These orientations can be determined by setting $dH/d\theta = 0$. For the $(\pm 3/2 \Leftrightarrow \pm 1/2)$ transitions only the perpendicular and parallel orientations are important so that equation 6 reduces to quite a simple set of equations.

$$Z_{34},\ H_{\text{par}}\left(+\frac{3}{2} \Leftrightarrow +\frac{1}{2}\right) = H_0 - \frac{2D}{g\beta} \qquad (7)$$

$$Z_{12},\ H_{\text{par}}\left(-\frac{1}{2} \Leftrightarrow -\frac{3}{2}\right) = H_0 + \frac{2D}{g\beta} \qquad (8)$$

$$XY_{34},\ H_{per}\left(+\frac{3}{2}\Leftrightarrow+\frac{1}{2}\right)=H_0+\frac{D}{g\beta} \quad (9)$$

$$XY_{12},\ H_{per}\left(-\frac{1}{2}\Leftrightarrow-\frac{3}{2}\right)=H_0-\frac{D}{g\beta} \quad (10)$$

(The symbols in the left-hand margin identify the transitions marked in figs. 6 and 7.) For the $M=(1/2\Leftrightarrow-1/2)$ transition an additional orientation near 42° provides a maximum field value.

$$Z_{23},\ H_{par}\left(+\frac{1}{2}\Leftrightarrow-\frac{1}{2}\right)=H_0 \text{ weak transition} \quad (11)$$

$$XY_{23},\ H_{per}\left(+\frac{1}{2}\Leftrightarrow-\frac{1}{2}\right)=H_0-\frac{0.75D^2}{g^2\beta^2H_0} \quad (12)$$

$$E_{23},\ H_{42°}\left(+\frac{1}{2}\Leftrightarrow-\frac{1}{2}\right)=H_0+\frac{1.33D^2}{g^2\beta^2H_0} \quad (13)$$

The spectrum thus has the characteristic form shown in fig. 7a. Note that the splitting of the two strong $1/2\Leftrightarrow-1/2$ peaks depends on D^2; the outer transitions are linear in D.

Orthorhombic symmetry. When the symmetry is lower than axial, there is an orthorhombic component to the crystal field and this is defined by the parameter E. A formula equivalent to equation 6 has been given by Low [37] and quoted elsewhere [7]; this equation is incorrect. However, equations for the x, y and z directions are relatively easy to calculate.

$$Z_{34},\ H_z\left(+\frac{3}{2}\Leftrightarrow+\frac{1}{2}\right)=H_0-\frac{2D}{g\beta}+\frac{3E^2D}{g\beta}\left[\frac{1}{(g\beta H)^2-D^2}\right] \quad (14)$$

$$Z_{23},\ H_z\left(+\frac{1}{2}\Leftrightarrow-\frac{1}{2}\right)=H_0-3E^2H\left[\frac{1}{(g\beta H)^2-D^2}\right] \quad (15)$$

$$Z_{12},\ H_z\left(-\frac{1}{2}\Leftrightarrow-\frac{3}{2}\right)=H_0+\frac{2D}{g\beta}-\frac{3E^2D}{g\beta}\left[\frac{1}{(g\beta H)^2-D^2}\right] \quad (16)$$

The value of H required for the correction term on the right-hand side of the equation is the same as that on the left. The values of H_x and H_y are obtained by substituting E by $(\pm E+D)/2$ and D by $(\pm 3E-D)/2$ (the upper and lower sign applying for x and y respectively). The equations hold with reasonable accuracy for $D<1/3\,g\beta H$. They are very useful for matching up observed spectra with existing data obtained from single crystals.

Fig. 7b shows a spectrum of Cr^{3+} in weak field with a slight orthorhombic distortion.The special point of interest in the spectra of figs. 7a and b is that they were both obtained from the same specimen but at different temperatures. They reveal the presence of a phase transition in $CH_3NH_3Al(SO_4)_2.12H_2O$ between 290 and 77° K. Previous observations [38] by epr have shown that this transition occurs at 157° K. Epr can equally well be used to follow the course of phase changes and of solid state reactions. As already pointed out in section 2.1.2, it is often possible to detect the existence of a phase by the presence of a characteristic spectrum from a suitable ion, even when the phase is well below the detection limit for X-ray diffraction [35].

3.2.2. Cr^{3+} in Strong Crystal Fields

The simple formulae of equations 6 to 16 break down when the crystal field is strong. Fortunately van Reijen [39] has devised a method in which the observed spectrum can be compared with charts computed for a wide range of values of D and selected values of E/D.

It commonly happens that D is large compared with $g\beta H$ and for such cases the spectrum is once more simplified, especially if $E=0$ or $\frac{1}{3}D$. For $E=0$ (axial symmetry) the spectrum is dominated by a peak at $H/H_0=0.52$; for $E=1/3$ (maximum orthorhombic distortion) $H/H_0=0.365$. This again points to the fact that epr is very dependent on the symmetry of centres and hence deductions about their environment and their location relative to compensating ions can often be made from a cursory examination of the spectrum.

3.2.3. Fe^{3+}

Because Fe^{3+} has five unpaired electrons, there are six possible energy levels in a magnetic field, moreover they are perturbed not only by the non-cubic fields defined by D and E but also by cubic crystal fields. When D and E are small, the fields for resonance can readily be calculated by a set of equations, equivalent to equations 14 to 16, given in a paper by Manoogian, Holuj and Carswell [40]. This paper also contains some diagrams equivalent to fig. 6 and other helpful information.

When D and E are large the cubic crystal field

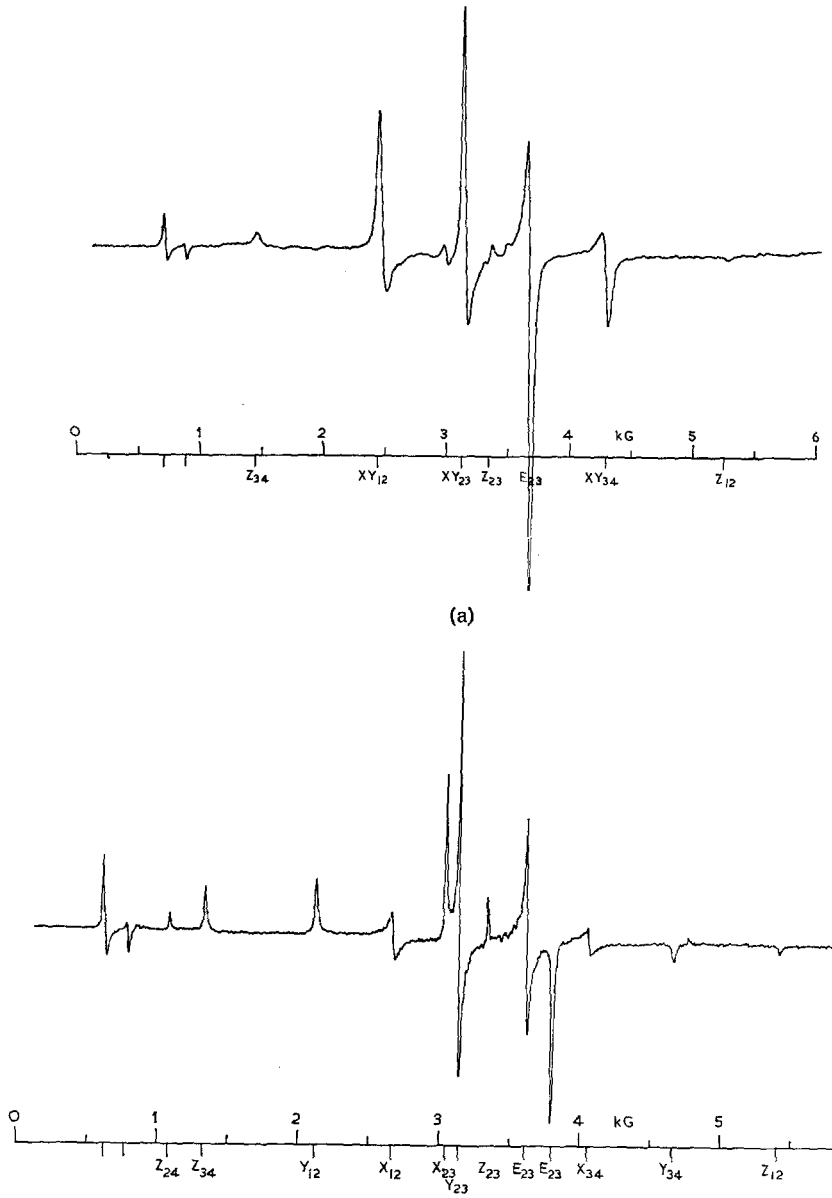

Figure 7 (a) The spectrum from Cr^{3+} in polycrystalline $CH_3NH_3Al(SO_4)_2.12H_2O$ at 293° K. Microwave frequency 0.309 cm^{-1}, $g = 1.973$, $D = 0.088$ cm^{-1}. From equations 7 to 13 it can be seen that the field intervals Z_{12} to Z_{34}, XY_{34} to XY_{12} and E_{23} to XY_{23} correspond to $4D/g\beta$, $2D/g\beta$ and $2.08\ D^2/g^2\beta^2H_0$ respectively. *E* indicates orientations other than X, Y or Z; (b) the spectrum from the same material but at 77° K. Microwave frequency 0.309 cm^{-1}. Baker [38] gives $D = 0.0958$ cm^{-1}, $E = 0.0092$ cm^{-1}, $g = 1.977$. Note how the XY peaks of fig. 7*(a)* separate into X and Y components and also note the correspondence of this spectrum with fig. 6. The parameters can be evaluated with the aid of equations 14 to 16.

is relatively unimportant so that it becomes possible to use computed charts for which only the non-cubic fields are considered. A set of these has been prepared by the author [41]. As with Cr^{3+}, characteristic, simplified spectra are obtained if D is very large and $E = 0$ or 1/3. The fields for the dominant resonance are then $H/H_0 = 1/3$ and 0.467 respectively. The way this simplification occurs can be seen from fig. 8 in which the resonance fields H/H_0 are plotted against E/D.

Experimental observations for Fe^{3+} in rutile plotted in the same figure show how the spectrum from polycrystalline material can be checked against existing single crystal data [42]. Fig. 6 is plotted for $D/h\nu > 2$ but fair agreement is obtained for $2 > D/h\nu > 1$.

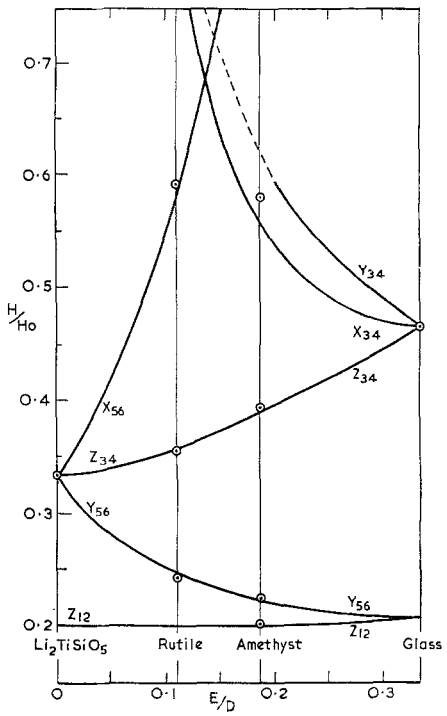

Figure 8 A chart to assist analysis of epr of Fe^{3+} in strong crystal fields. The fit is good for $D/h\nu > 2$ and fair for $2 > D/h\nu > 1$. Experimental points are shown for polycrystalline rutile, $D^2h\nu = 2.2$ and for amethyst single crystals, $D/h\nu = 0.98$. The values of D for Fe^{3+} in glass and Li_2TiSiO_5 are not known. The Y_{56} and Z_{12} transitions at fields below $H/H_0 = 0.23$ are very weak [41].

3.2.4. Mn^{2+}

Mn^{2+} is the most suitable transition metal ion to use as a monitor of the likely behaviour of divalent ions (Mg^{2+}, Zn^{2+}) in various hosts. This is so because having a half-filled *d*-shell it is spherically symmetrical, has no crystal field stabilisation energy and does not cause strong distortion of its surroundings. The only natural isotope is ^{55}Mn, which has a nuclear spin of 5/2. The resultant hyperfine structure in the spectra can be very complex but the effort of interpretation is rewarded by the fact that the nuclear spin coupling parameter is linearly related to the percentage ionic character of the bond [43, 44]. An additional advantage of using Mn^{2+} as a monitor ion is that its co-ordination may also be determined by optical fluorescence spectroscopy [45].

A description of the epr of Mn^{2+} in polycrystalline material (almost certainly calcite [46] in modelling clay) has been given in a very clear account by Bleaney and Rubins [47]. The use of Mn^{2+} as a monitor of cation distribution in polycrystalline and amorphous materials has been described for zeolites [48], glasses [49, 50] and for a study of the formation of fluorapatite [51]. The work of Griscom and Griscom [50] on Mn^{2+} in borate glasses is an example of how patient interpretation of spectra has been used to gain an understanding of a material, in this case of the degree of variation of types of ionic environment in a glass.

3.3. Line Width and Exchange Coupling

There are two important sources of line broadening which are discussed briefly below; fuller reviews are given by Kokoszka and Gordon [7], König [8] and Orton [9].

3.3.1. Relaxation Broadening

Increased uncertainty of the energy levels of the spin states is caused by rapid spin-lattice or spin-spin relaxation, which shorten the lifetime of the electrons in the energy levels. Spin-spin relaxation is dependent on concentration, whereas spin-lattice relaxation is dependent on symmetry and temperature. If the spin-lattice relaxation is too fast, loss of intensity results through line broadening; if it is too slow, then a phenomenon known as saturation also reduces intensity, either with no change in line shape or with loss of the centre of the peak. The saturation is dependent on the temperature and microwave power level so that control of these factors often enables superimposed spectra to be resolved.

3.3.2. Inhomogeneity Broadening

Variations in the environment and orientation of paramagnetic centres cause line broadening as already touched upon in sections 2.1.3, 3.1.3, and 3.2.4. This source of line broadening is particularly prominent in amorphous materials.

3.3.3. Spin Dipole Interaction

The magnetic dipole of an unpaired electron aligned in a magnetic field produces its own local field which adds to or subtracts from the field felt by neighbouring unpaired electrons. This local field amounts to 300G at a distance of 4Å

[7]. Thus, if the concentration of paramagnetic ions is high there is an almost continuous distribution of local field strengths and the effect of spin dipole interaction is seen as considerable line broadening. However, at intermediate concentrations resolved satellites can be seen surrounding the transitions from magnetically isolated ions [52].

3.3.4. Exchange Coupling

Exchange coupling is more specific and structure sensitive [53] than the spin dipole interaction discussed above. If the wave functions of two unpaired electrons interact with an exchange energy, J, greater than $g\beta H$ then they no longer behave independently but couple to form a single spin system. They form what is essentially a weak molecule. If J is positive (antiferromagnetic exchange), the ground state of the system is diamagnetic, $S = 0$, but there is an excited state with $S = 1$, which is populated according to a Boltzmann distribution. An applied magnetic field splits the three spin levels of the excited state and epr can be observed with a temperature dependence characteristic of J. The resonance field is influenced by dipolar interaction, anisotropic exchange, crystal field strength and nuclear spin coupling, but often occurs near H_0.

When antiferromagnetic exchange occurs between two unlike ions with non-integral total spin, for example between Fe^{2+} and Fe^{3+}, the ground state is paramagnetic with spin 1/2 and the resonance intensity should increase with decreasing temperature.

In magnetically concentrated, antiferromagnetic materials such as Cr_2O_3, the exchange coupling is co-operative and consequently has a characteristic transition temperature which is denoted T_N, the Néel temperature. For Cr_2O_3 T_N is 307° K; below this temperature epr does not occur [54], but above T_N the spins, although they do not behave independently, become more like pairs and epr is seen as a broad resonance centred near H_0 and with a typical line width of 400 gauss, dependent on particle size [55].

The potential power of studies of exchange interactions is revealed by the work of Statz *et al* [52], who were able to assign the resonance from Cr^{3+} pairs in Al_2O_3 up to the eleventh nearest neighbours, which are 5.73Å apart. The technique could be used to examine the early stages of nucleation of precipitates of one crystalline phase within another. For example, a component in the epr spectra of Mn^{2+} in NaCl has been tentatively assigned to a Mn^{2+} trimer [20]. Exchange coupling has been used by Landry, Fournier and Young [56] to investigate clustering of Cr^{3+} ions in a phosphate glass and extensively by workers on chromia-alumina catalysts [57].

4. Practical Aspects

In electron spin resonance spectrometers, the specimen is held in a microwave cavity, where it is exposed to radiation at X-band (9 to 10 GHz), K-band (23 GHz) or Q-band (35 GHz). As described in section 3.1, the spectrum is obtained by varying the magnetic field at the specimen. Usually the magnetic field is modulated at 100 KHz and a phase sensitive detection system provides a first derivative presentation of the absorption spectrum. Design features are discussed by Poole [58] and Wilmshurst [59].

The spectrometer should preferably have either a fixed or a measured microwave frequency. For use with an X-band spectrometer (9 to 10 GHz) it is essential to have a magnet whose field can be varied from 0 to 6 kG or to higher values and for which the automatic field sweep can cover the entire field range. The sweep should be free of jerks, caused for example by the jumps between successive wires in a potentiometer. It is desirable to be able to record the spectra on an X-Y recorder as a linear function of field so that spectra can be compared directly.

Observations at liquid nitrogen temperature with a thin-tailed Dewar within the cavity are often impeded by boiling of the nitrogen which detunes the spectrometer. A stream of helium bubbled through hypodermic tubing just above the microwave cavity level prevents boiling within the cavity. The use of a range of temperature to differentiate spectra components has already been noted. Normal behaviour is that the intensity of the spectrum should increase as T^{-1} unless saturation or exchange coupling occur. Facilities for continuous variation of the temperature from 77° to 600° K are most desirable for observation of exchange phenomena.

If as often happens there is any difficulty about interpretation of spectra it may be easier to prepare other specimens with modified composition so that trends in the spectra can be followed. This procedure often allows components of the spectra to be differentiated and identified with the bonus of further experimental information.

The optimum concentration of paramagnetic

centres within single crystals is 10^{-4} centres/atom of matrix but up to 10^{-3} or even 10^{-2} may be tolerated before really serious line broadening occurs. Information is still available, especially about magnetic exchange, even if the concentration is very high.

The measurement of the resonance intensity in order to measure concentrations is not simple in practice. Usually a comparative method is employed [60]. Epr cannot be guaranteed to discover all paramagnetic ions present in the specimen, for example some centres may have very rapid spin-lattice relaxations. A particular difficulty in amorphous specimens is that at any particular microwave frequency the sensitivity is a function of the crystal field strength, so a false idea of the distribution of field strengths can easily be obtained.

5. Summary

An understanding of the effect of impurities on the fabrication and performance of materials can be achieved only if the location of the impurities is known. Epr can be used to investigate this influence on a wide range of the properties of materials. Examples are given of its relevance to observations of phase change, crystal growth, nucleation, catalysis, glass structure, local and general mechanical strain and cation distribution.

Methods are briefly described for analysis and interpretation of spectra. Careful interpretation of spectra can give detailed information about the paramagnetic centres and their environment but even a cursory examination of the spectra will often reveal useful information, especially if variations are studied over a range of specimens.

One of the most promising developments for applications of epr in materials research is the use of exchange coupling to detect the initial stages of ion clustering in crystals, or phase separation on grain-boundaries and in glasses. Epr can be used most powerfully in materials research when it is coupled with exploration by a wide range of other techniques, such as electron microscopy and electron probe microanalysis.

Acknowledgement

The author gratefully thanks Dr R. Wilson for producing the computed spectrum of fig. 5.

Glossary

S = electron spin = 1/2 × number of unpaired electrons.
M = component of the spin along the axis of quantisation. Takes values from $+S$ to $-S$.
I = nuclear spin.
m = nuclear spin component, takes values from $+I$ to $-I$.
g = spectroscopic splitting factor.
β = Bohr magneton.
h = Planck's constant.
ν = microwave frequency.
H = magnetic field (strictly magnetic induction B should be used) 1 Gauss = 10^{-4} Tesla.
$H_0 = h\nu/g\beta$, $H_{0\,par} = h\nu/g_{par}\beta$ etc.
W = difference in energy between the individual spin states and their mean energy.
A = parallel nuclear spin coupling energy*.
B = perpendicular nuclear spin coupling energy*.
D = axial crystal field energy*. Other equivalent symbols are $b_2^0 = D = 3B_2^0$.
E = orthorhombic crystal field energy*. Other equivalent symbols are $\frac{1}{3}b_2^2 = E = B_2^2$.
J = exchange coupling energy.

References

1. F. C. FRANK, Proc. Intern. Industrial Diamond Conf. Oxford, 1966 (Industrial Diamond Information Bureau, London, 1967) p. 119.
2. V. S. STUBICAN and D. VIECHNICKI, *J. Appl. Phys.* **37** (1966) 2751.
3. R. C. HALL, *Ceram. Bull.* **47** (1968) 251.
4. J. H. WELCH and W. GUTT, 4th Intern. Symp. Chemistry of Cement, Washington DC, 1960, p. 59.
5. A. CARRINGTON and H. C. LONGUET-HIGGINS, *Quart. Rev. Chem.* **14** (1960) 427.
6. W. LOW and E. L. OFFENBACHER, *Solid State Phys.* **17** (1966) 135.
7. G. F. KOKOSZKA and G. GORDON, "Technique of Inorganic Chemistry", Vol. 7, edited by H. B. Jonassen and A. Weissberger (Interscience, J. Wiley, 1968) p. 151.
8. E. KÖNIG, "Physical Methods in Inorganic Chemistry", edited by H. A. O. Hill and P. Day (Interscience, J. Wiley, 1968) p. 266.
9. J. W. ORTON, "Electron Paramagnetic Resonance" (Iliffe, London, 1968).
10. H. J. GERRITSEN, "Symposium on Paramagnetic Resonance (1962)", Vol. 1, edited by W. Low (Academic Press, New York, 1963) p. 3.
11. T. I. BARRY, *Solid State Commun.* **4** (1966) 123.
12. W. M. WALSH JR, *Phys. Rev.* **122** (1961) 762.
13. E. R. FEHER, *ibid* **136** (1964) A145.
14. A. M. STONEHAM, *Proc. Phys. Soc.* **89** (1966) 909; *J. Phys. C. (Proc. Phys. Soc.)* Ser. 2 **1** (1968) 565;

*The parameters A, B, D and E can also be expressed in units of gauss. For example A (in gauss) = A (in energy)/$g\beta$. This is often done to simplify the form of equations 3 to 16.

UKAEA Report AERE-R5530; *Rev. Mod. Phys.* (Jan 15 1969).
15. A. J. BURGGRAAF and J. CORNELISSEN, *Phys. Chem. Glasses* **5** (1964) 123.
16. H. P. KIRCHNER, R. M. GRUVER, and R. E. WALKER, *J. Amer. Ceram. Soc.* **51** (1968) 251.
17. R. F. WENZEL and Y. W. KIM, *Phys. Rev.* **140** (1965) A1592.
18. C. J. KIRKBY and J. S. THORP, *J. Phys. C. (Proc. Phys. Soc.)* **1** (1968) 913.
19. J. J. RASMUSSEN, G. B. STRINGFELLOW, I. B. CUTLER, and S. D. BROWN, *J. Amer. Ceram. Soc.* **48** (1965) 146.
20. H. F. SYMMONS and R. C. KEMP, *Brit. J. Appl. Phys.* **17** (1966) 607.
21. G. D. WATKINS, *Phys. Rev.* **113** (1959) 79, 91.
22. P. L. PRATT, *Proc. Brit. Ceram. Soc.* 1 (1964) 177 J. P. ESHELBY, C. W. A. NEWEY, P. L. PRATT, and A. B. LIDIARD, *Phil. Mag.* **3** (1958) 75.
23. G. BLASSE, *Philip's Res. Rep. Suppl.* No. 3 (1964).
24. F. A. KROGER, "The Chemistry of Imperfect Crystals" (North Holland, Amsterdam, 1964).
25. W. A. DEER, R. A. HOWIE, and J. ZUSSMAN, "Rock Forming Minerals", Vols. 1-4 (Longmans, London, 1962).
26. J. H. MACKEY, JR, *J. Chem. Phys.* **39** (1963) 74.
27. Y. HAVEN, A. KATS, and J. S. VAN WIERINGEN, *Philips Res. Rep.* **21** (1966) 446.
28. T. I. BARRY, P. MCNAMARA, and W. J. MOORE, *J. Chem. Phys.* **42** (1965) 2599.
29. S. GESCHWIND and J. P. REMEIKA, *Phys. Rev.* **122** (1961) 757.
30. S. A. MARSHALL and A. R. REINBERG, *ibid* **132** (1963) 134.
31. F. K. KNEUBÜHL, *J. Chem. Phys.* **33** (1960) 1074.
32. J. W. SEARL, R. C. SMITH, and S. J. WYARD, *Proc. Phys. Soc.* **A78** (1961) 1174.
33. T. VÄNNGÅRD and R. AASA, "Symposium on Paramagnetic Resonance (1962)", edited by W. Low, Vol. 2, (Academic Press, New York, 1963) p. 509.
34. B. BLEANEY, *Phil. Mag.* **42** (1951) 441.
35. T. I. BARRY, and L. A. LAY, "6th Intern. Symp. Reactivity of Solids, Schenectady (1968)" (J. Wiley, New York, 1969).
36. H. G. HECHT and T. S. JOHNSTON, *J. Chem. Phys.* **46** (1967) 23.
37. W. LOW, *Solid State Phys.* Suppl. 2 (1960).
38. J. M. BAKER, *Proc. Phys. Soc.* **B69** (1956) 633.
39. L. L. VAN REIJEN, Thesis, Technological University Eindhoven (1964).
40. A. MANOOGIAN, F. HOLUJ, and J. W. CARSWELL, *Canad. J. Phys.* **43** (1965) 2262.
41. T. I. BARRY, NPL Report, IMU Ex 6 (1967).
42. D. L. CARTER and A. OKAYA, *Phys. Rev.* **118** (1960) 1485.
43. J. S. VAN WIERINGEN, *Disc. Far. Soc.* **19** (1955) 118.
44. J. C. M. HENNING, *Phys. Lett.* **24A** (1967) 40.
45. K. BINGHAM and S. PARKE, *Phys. Chem. Glasses* **6** (1965) 224.
46. F. K. HURD, M. SACHS, and W. D. HERSHBERGER, *Phys. Rev.* **93** (1954) 373.
47. B. BLEANEY and R. S. RUBINS, *Proc. Phys. Soc.* **77** (1961) 103 corrected **78** (1961) 778.
48. T. I. BARRY and L. A. LAY, *J. Phys. Chem. Solids* **27** (1966) 1821; **29** (1968) 1395.
49. H. W. DE WIJN and R. F. VAN BALDEREN, *J. Chem. Phys.* **46** (1967) 1381.
50. D. L. GRISCOM and R. E. GRISCOM, *ibid* **47** (1967) 2711.
51. J. A. PARODI, *J. Electrochem. Soc.* **114** (1967) 370.
52. H. STATZ, L. RIMAI, M. J. WEBER, G. A. DE MARS, and G. F. KOSTER, *J. Appl. Phys.* Suppl. 32 (1961) 218S.
53. J. OWEN, *J. Appl. Phys.* Suppl. 32 (1961) 213S; *J. Appl. Phys.* Suppl 33 (1962) 355S.
54. T. R. MCGUIRE, E. J. SCOTT, and F. H. GRANNIS, *Phys. Rev.* **102** (1956) 1000.
55. C. P. POOLE and J. F. ITZEL, *J. Chem. Phys.* **41** (1964) 287.
56. R. J. LANDRY, J. R. FOURNIER, and C. G. YOUNG, *ibid* **46** (1967) 1285.
57. C. P. POOLE and D. S. MACIVER, "Advances in Catalysis", Vol. 17 (Academic Press, New York, 1967) p. 223.
58. C. P. POOLE, "Electron Spin Resonance" (J. Wiley, New York, 1966).
59. T. H. WILMSHURST, "Electron Spin Resonance Spectrometers" (Hilger & Watts, London, 1967).
60. L. S. SINGER, *J. Appl. Phys.* **30** (1959) 1463.